Thermal transport studies of 351-nm laser-produced plasmas using extreme ultraviolet spectroscopy

J. C. Moreno, H. R. Griem, S. Goldsmith,[a] and A. Krumbein[b]
Laboratory for Plasma and Fusion Energy Studies, University of Maryland, College Park, Maryland 20742

R. Epstein, P. A. Jaanimagi, M. C. Richardson, and B. Yaakobi
Laboratory for Laser Energetics, University of Rochester, 250 East River Road, Rochester, New York 14623

(Received 24 July 1987; accepted for publication 2 October 1987)

Spectra from an extreme ultraviolet (XUV) grazing incidence spectrograph have been used in the study of thermal transport in laser plasmas. These measurements with XUV lines allowed a diagnosis of much lower temperatures in the heating front than had been previously measured. The OMEGA (24-beam, 351-nm) laser system at the University of Rochester was used to produce plasmas from glass microballoons coated with Al or Ti substrates and overcoated with a plastic ablator. Thermal transport was investigated by measuring the intensity of x-ray and XUV lines as a function of the thickness of the plastic overcoat. These measurements were then compared to the 1D hydrodynamic code LILAC. Agreement between the hydrodynamic code and experiment could not be obtained with a reasonable value for the flux limiter ($f \leqslant 0.65$). Consistent results were reached if nonuniform irradiation and flux inhibition is assumed. The measured burnthrough depths of around 9 μm are similar to previous measurements made with x-ray lines at fluxes below 10^{15} W/cm^2. No evidence of preheat in the heat front was observed.

I. INTRODUCTION

Experimental studies of electron heat transport are essential to an understanding of laser-plasma behavior.[1,2] In a laser-driven ablating plasma the laser energy is absorbed in the corona near the critical density layer and transported inward by the electron heat flow. Inward penetration of this heat flux determines the resulting plasma temperature profile. In addition, a large inward heat flux will cause the surface of the cold dense inner region to expand outward rapidly. Recoil momentum from this outward expansion will in turn further compress the dense inner part of the target. Energy transport by radiation cannot be neglected and under some conditions (e.g., low irradiance, long pulse length), it can play a dominant role in ablating plasmas.[3] The production of high-energy radiation and hot electrons, resulting in preheat, will also influence the ablation process.

Electron heat transport can be examined indirectly through spectroscopic and charge collector measurements. In general, targets with low Z overcoats of different thicknesses are used to study the penetration of the heat flux into higher Z signature emitting layers. In laser-produced plasmas, it has been found that the measured heat flux is much less than the value predicted classically by Spitzer and Härm.[4] The Spitzer–Härm model of the electron heat flux is usually modified by applying an upper limit given by the expression

$$Q_f = f n_e k T_e (k T_e / m_e)^{1/2},$$

where n_e is the electron density, T_e is the electron temperature, m_e is the electron mass, and f is referred to as the flux limiter.[5–7] For electrons free streaming in a vacuum the value of f is near unity. However, simulations of laser-plasma experiments require values of the flux-limiter generally much less than one.

Early experiments on thermal transport used planar targets and measured the flux-limiter to be in the range $0.03 < f < 0.1$.[8–10] The importance of using short wavelength lasers for ablative compression was quantified[10] by measuring mass ablation rates at three different laser wavelengths. Planar target experiments were difficult to model because of the two-dimensional geometry. Consequently, the next experiments[11–13] switched to spherical targets allowing more direct comparisons to be made to simpler one-dimensional theoretical models. Thermal transport in these experiments could also generally be modeled with a flux limiter less than 0.1, except for an experiment[11] in which for $\lambda = 530$ nm, a flux limiter of $f > 0.1$ was required.

Experiments at LLE[14,15] showed a much more efficient thermal transport than measured with single-beam irradiation. In the 1054-nm laser irradiation experiments[14] measurements indicated the presence of a low-temperature foot ahead of the heat front. The burnthrough curves could not be modeled with any flux-inhibited model. With 351 nm, 6-beam laser irradiation onto spherical targets[15] no evidence of a low-temperature foot was observed although radiative preheat was seen. Mass ablation rates were found to be higher than with 1054-nm irradiation. Again very deep burnthrough was observed which did not agree with flux-inhibited transport. Recently it has been shown that nonuniformity of the laser irradiation and flux inhibited transport is suffi-

[a] Permanent address: School of Physics and Astronomy, Tel Aviv University, Tel Aviv 69978, Israel.
[b] Permanent address: Plasma Physics Department, Israel Atomic Energy Commission, Soreq Nuclear Research Center, Yavne 70600, Israel.

 0021-8979/88/030674-07$02.40

cient to account for the discrepancy between measured and predicted burnthrough.[16,17]

Previous studies of thermal transport relied upon x-ray line emission which probes the hotter regions of the ablating plasmas ($T_e > 500$ eV). In this study, in addition to the usual x-ray spectroscopy, we have also performed extreme ultraviolet (XUV) measurements of highly ionized high Z ions. These measurements have a broader emission wavelength coverage and look at a much lower and wider temperature region of the plasma ($60 < T_e < 1500$ eV) than previous measurements. This is important for studying thermal transport from the ablation front to the critical density layer. It can also shed additional light on questions of preheat and the shape of the temperature profile. Heat conduction is inferred here from the measured penetration depth of the laser-driven thermal fronts in spherical targets and from comparisons to a hydrodynamic code (LILAC). The measured burnthrough depths indicate a thermal front with no hot electron preheat or low-temperature foot. As in previous spherical geometry experiments at LLE, it was found that the burnthrough depth was inconsistent with a flux-inhibited model. Using a larger effective irradiance in the model to account for nonuniform irradiance (hot spots) gave good agreement between experiment and code.[17]

Section II contains a description of the experimental arrangement, including the laser system, targets, spectrograph, and additional diagnostics. In Sec. III the experimental results are shown and analyzed. Section IV has a discussion of the results along with a comparison to a hydrocode (LILAC). Finally, Sec. V contains a summary and conclusions.

II. EXPERIMENTAL DESCRIPTION

Plasma spectroscopic measurements in the extreme ultraviolet were performed with a 3-m grazing incidence spectrograph. The spherical ablation plasmas used for these measurements were produced with the OMEGA laser system at the Laboratory for Laser Energetics (LLE) at the University of Rochester. The laser system is comprised of 24 beams frequency tripled to a wavelength of 351 nm. Typical incident intensities used for this investigation were 4×10^{14} W/cm^2, while the pulse length was 600 ps. Focusing the laser light at 8 times the target radius beyond the target center provided optimum uniformity.

The spherical targets consisted of glass microballoons, 400 μm in diameter and approximately 10 μm in wall thickness (Fig. 1). These microballoons were coated with a 2-μm layer of either Al or Ti to provide signature line emission. A final overcoat (0–11 μm) of parylene was deposited on the targets. Using targets with different overcoat thicknesses was crucial to the thermal transport study since measurements of line intensity as a function of plastic overcoat thickness were used in the analysis. Aluminum targets also contained oxygen and nitrogen impurities due to the pulsed nitrogen process employed for sputter coatings of Al onto glass microballoons.[18]

The principal diagnostic for these measurements was a grazing incidence XUV spectrograph.[19] Radiation from the

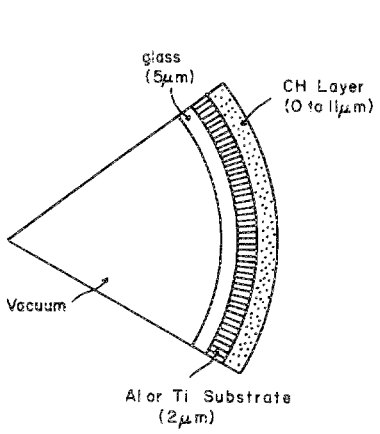

FIG. 1. Drawing of a typical spherical target used for these measurements.

plasma was focused onto the entrance slit of the spectrograph with a cylindrical concave mirror. This mirror was positioned at a grazing angle of incidence to the incoming light and had an adjustable radius of curvature to focus the light. The spectrograph employed an 88° incidence angle and contained a 1200 lines/mm grating blazed at 2° 35′, giving a peak efficiency at 60 Å. Other diagnostics that were also operating during these experimental runs include time-integrated x-ray crystal spectrographs, an x-ray streak camera, and plasma calorimeters. Time histories of H-like and He-like Al were measured using a twin channel streak camera/photographic camera elliptical analyzer x-ray spectrograph (SPEAXS).[20]

Time-integrated spectra were recorded on photographic plates with the grazing incidence spectrograph. Although the spectrograph lacked time resolution it had the advantage of covering a large wavelength range. The photographic plates were 10-in.-long Kodak-type 101-05 plates covering the spectral region between 6 and 70 Å. The principal lines of interest in this region were emission lines from Li-like ions of Al and Ti. A typical spectrum for a target coated with Al (2 μm) and CH (3 μm) is shown in Fig. 2. Similarly, a Ti (2 μm) and CH (3 μm) spectrum is shown in Fig. 3. Spectra were digitized and stored on a computer using a Perkin–Elmer microdensitometer.

A relative calibration of the 101-05 plates was performed using a 2.2-m grazing incidence spectrograph attached to a University of Maryland theta pinch. Several spectra from theta pinch produced argon plasmas were recorded on each photographic plate. Each of the spectra was for a different exposure time corresponding to different numbers of integrated plasma shots. The calibration plates were carefully developed under the same conditions as the experimental data. This allowed the relative intensity of the emission lines to be related to the optical density on the plates. It is estimated that the error in the calibration is less than 20%.

III. EXPERIMENTAL RESULTS

Relative intensities of emission lines, in the wavelength region covered by the spectrograph, were determined for

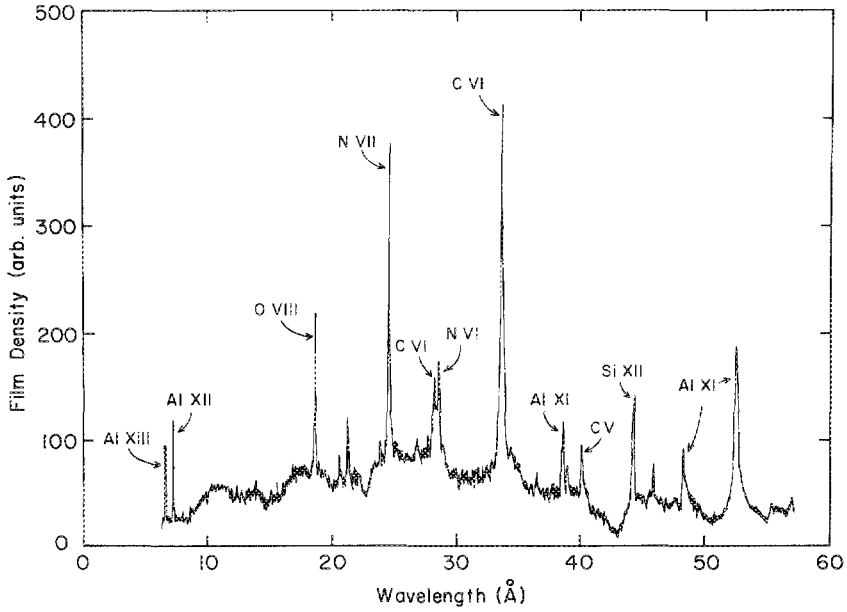

FIG. 2. Time-integrated spectrum from a target coated with 2 μm of Al and 3 μm of CH.

each plasma shot. These emission lines resulted from the ionization of the outer layers of the target, namely, the metallic substrate layer (Al or Ti) and the parylene coating (CH). Impurities in the Al targets also resulted in N and O emission. Table I contains a list of the XUV emission lines which were used in this investigation.

Al and Ti relative line intensities were plotted as a function of the thickness of the plastic coating (Figs. 4–6). A least-squares parabolic fit was made to the data to help indicate burnthrough depths. These emission lines exhibit a decrease in intensity as the thickness of the plastic layer increased. This decrease results from the increasingly thick plastic layer consuming an increasing fraction of the laser energy, thus leaving less energy to heat the inner layers. The nonsteady nature of this decrease for plasma shots with Al substrates may be due to imperfect beam balance and shot-to-shot variations in laser intensity resulting in slightly different plasma conditions. The Al shots averaged 18% rms variation of the target laser energy of the 24 beams while the Ti shots which had much smoother burnthrough curves averaged only 9% rms variation. Another contributing effect ($<5\%$) could be slight differences in photographic plate development.

The thickness of the plastic at which the line intensity falls to approximately the background level is referred to as the burnthrough depth. Emission from Li-like ions of Al and Ti showed a burnthrough depth of 8–10 μm. Comparing the Li-like ion emission to H-like and He-like Al emission we see that there is no significant difference in the measured value of the burnthrough depth despite the large difference in temperature for the plasma regions in which these ions are principally located. Results from earlier experiments at LLE[15]

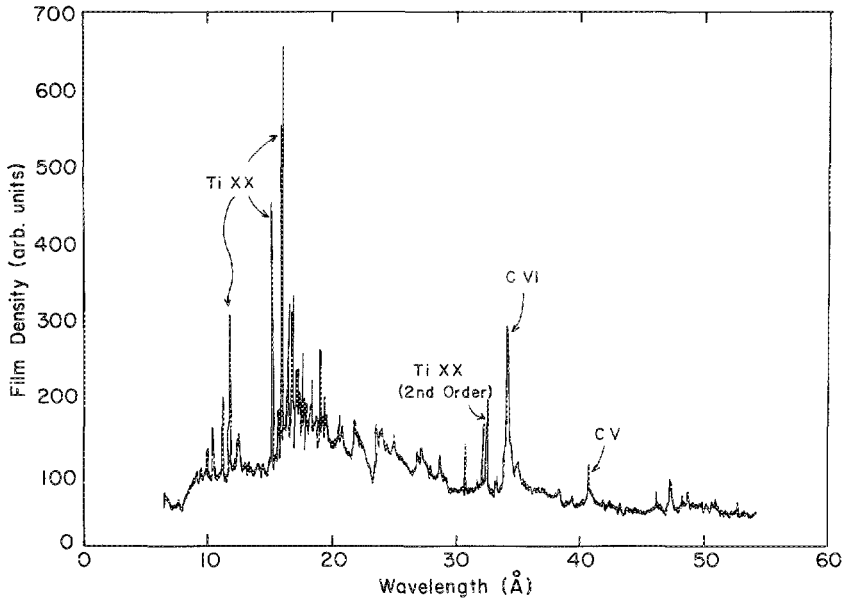

FIG. 3. Time-integrated spectrum from a target coated with 2 μm of Ti and 3 μm of CH.

TABLE I. Strong emission lines observed with the XUV spectrograph.

Ion	Transition	Wavelengths (Å)
AlXIII	$1s\ ^2S$-$2p\ ^2P$	7.173
AlXII	$1s^2\ ^1S$-$1s2p\ ^1P$	7.757
AlXI	$2p\ ^2P$-$4d\ ^2D$	39.091, 39.180
AlXI	$2s\ ^2S$-$3p\ ^2P$	48.297, 48.338
AlXI	$2p\ ^2P$-$3d\ ^2D$	52.299, 52.446
TiXX	$2p\ ^2P$-$4d\ ^2D$	11.87, 11.94
TiXX	$2s\ ^2S$-$3p\ ^2P$	15.217, 15.252
TiXX	$2p\ ^2P$-$3d\ ^2D$	15.914, 16.059
CVI	$1s\ ^2S$-$3p\ ^2P$	28.466
CVI	$1s\ ^2S$-$2p\ ^2P$	33.736
CV	$1s^2\ ^1S$-$1s2p\ ^1P$	40.268
OVIII	$1s\ ^2S$-$2p\ ^2P$	18.969
NVII	$1s\ ^2S$-$2p\ ^2P$	24.781
NVI	$1s^2\ ^1S$-$1s2p\ ^1P$	28.787

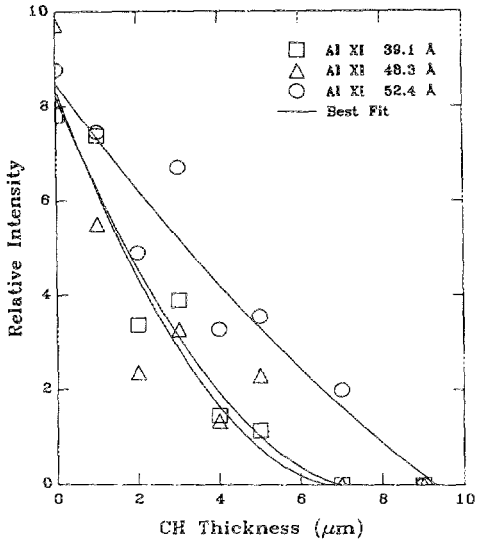

FIG. 5. Experimental measurements of Li-like Al-line emission as a function of CH thickness. $I_L \approx 3\times10^{14}$ W/cm^2.

using six beams exhibited similar burnthrough depths for H-like and He-like Al and Ti. In addition, measurements of N- and O-line emission (Fig. 7) also show a burnthrough depth nearly the same as Al and Ti ions. The range in temperature, for the plasma regions from which all these ions radiate in the XUV, is quite large ($60 < T_e < 1500$ eV). The average temperature at which the different charge states exist in these high-density plasmas can be determined to within 20% from a coronal model. If we plot the burnthrough depth as a function of the electron temperature for the different observed ions (Fig. 8), we see that there is no significant dependence of the measured burnthrough depth on the isotherm in the plasma which is probed. This indicates that the electron temperature falls slowly with CH thickness until the burnthrough depth is approached in which case it then falls rapidly. Note that our isotherm dependence result differs from a previous LLE experiment[14] using a longer wavelength laser system ($\lambda = 1054$ nm).

This lack of isotherm dependence also indicates that there is no evidence for hot electron preheat or any low-temperature foot ahead of the heat front. These effects would have been manifested through larger burnthrough depths for Li-like spectroscopic measurements. No significant preheat means the electron temperature profile is most likely smoothly varying and thermal flux for these plasma conditions can be described by flux-inhibited transport. The lack of measureable preheat can be explained by the shorter laser wavelength ($\lambda = 354$ nm) used here which leads to shorter scale lengths and increased inverse bremsstrahlung. In turn, fewer hot electrons are produced by resonant absorption.

The mass ablation rate can be calculated for this experiment using the following expression:

$$\frac{dm}{dt} = \frac{\rho \Delta r}{\Delta \tau},$$

where Δr is the burnthrough depth, ρ is the density of the

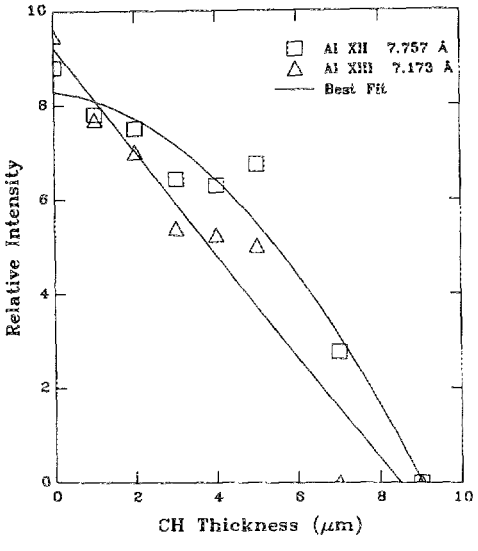

FIG. 4. Experimental measurements of H-like and He-like Al-line emission as a function of CH thickness. The burnthrough depth is around 9 μm. $I_L \approx 3\times10^{14}$ W/cm^2.

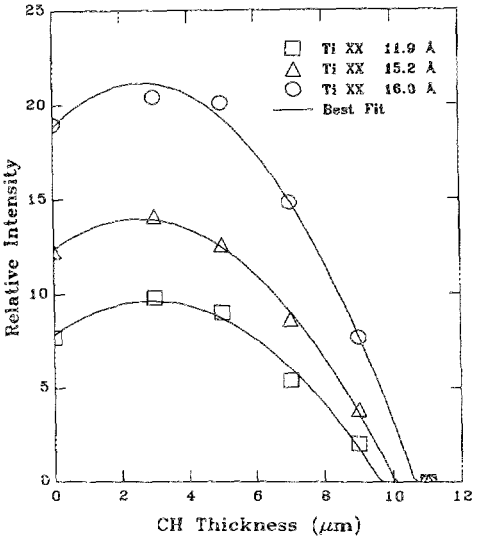

FIG. 6. Experimental measurements of Li-like Ti-line emission as a function of CH thickness. $I_L \approx 4.2\times10^{14}$ W/cm^2.

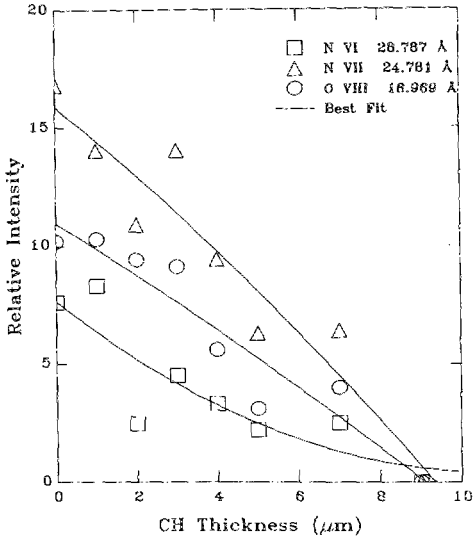

FIG. 7. Experimental measurements of impurity line emission as a function of CH thickness. $I_L \approx 3\times 10^{14}$ W/cm^2.

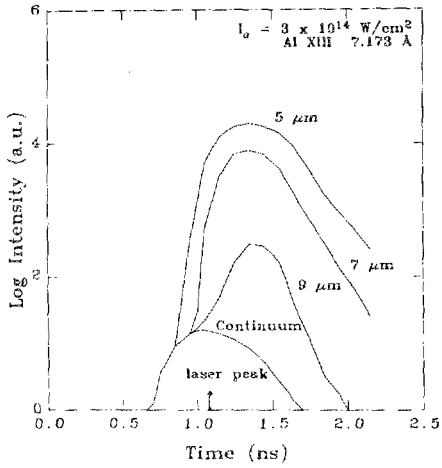

FIG. 9. Time history of H-like Al line emission using the SPEAXS x-ray streak camera system. Note how the peak of the emission is later in time as the CH thickness is increased.

plastic, and $\Delta\tau$ is the laser pulse width. For a laser intensity of 3×10^{14} W/cm^2 the mass ablation rate was typically found to be 1.7×10^6 g/cm^2 s. This value is consistent with previous results using time-integrated x-ray line emission.[15]

The SPEAXS x-ray streak camera took time-resolved measurements of the AlXIII ($1s$-$2p$) resonance line. Figure 9 shows time histories of AlXIII for different thicknesses of CH. The background continuum level is also indicated. For increasing CH thickness, the peak of the emission comes later in time because of the longer burnthrough path. The burnthrough rate, computed from the different initial times at which line emission begins to rise for different CH thicknesses, gives a mass ablation rate of 2.2×10^6 g/cm^2 s which is slightly higher than the value derived from time-integrated spectroscopic measurements. However, it is difficult to compare these measurements directly because nonuniformities in laser irradiation can affect the onset times for line emission.

An interesting result, which will be discussed in more detail elsewhere, is the behavior of C line emission with varying CH thicknesses. The CVI ($1s$-$2p$) and the CV ($1s^2$-$1s2p$) resonance lines show a saturation in line intensity as the CH thickness is increased. This is most likely due to the plasma being optically thick to these lines. The CVI Lyman-β line on the other hand may not be optically thick since it does not exhibit any saturation.

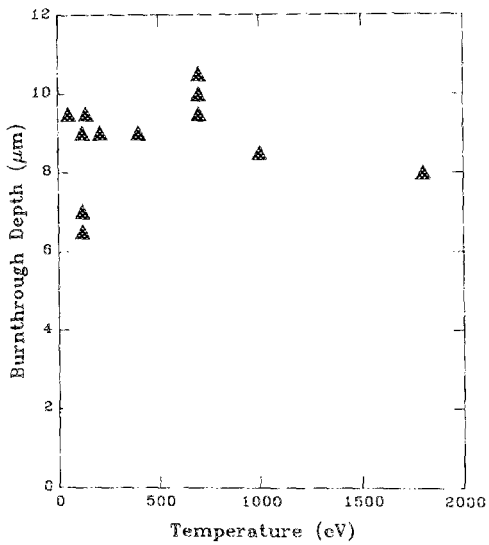

FIG. 8. Measured burnthrough depths for different ions plotted as a function of the electron temperature. The data for TiXXI is from Ref. 14.

IV. DISCUSSION

The interpretation of the present thermal transport study consists mainly of comparisons of spectroscopic measurements to theoretical simulations. We have used a one-dimensional Lagrangian hydrodynamics simulation code called LILAC.[21] This code uses a flux-limited Spitzer–Härm thermal transport, flux-limited multigroup diffusive radiation transport using LTE opacities from LASL astrophysical libraries and ray tracing of incident laser light with realistic focusing and beam profiles to compute the deposition of laser energy into the target by inverse bremsstrahlung. Temperature and density time histories from LILAC are then input into a non-LTE post-processor. Emissivities and opacities are computed from the solution of coupled atomic population equations and the equation of radiation transfer is solved for the emitted radiation over a finely resolved spectral grid. For this experiment it was necessary to add Li-like transitions to the post-processor.

Figure 10 shows a simulated burnthrough curve for targets with Al substrate and parylene overcoating. The burnthrough depth from this simulation, using a value $f = 0.1$, does not match with experimental data. Raising the flux-limiter within plausible bounds ($f \leqslant 0.65$) does not improve the agreement sufficiently. Figure 11 shows the scaling of simulated AlXI line emission with the flux-limiter. Above $f = 0.1$ there is little effect on line intensity.

The much larger burnthrough depth measured in the experiment is most readily explained by taking into account

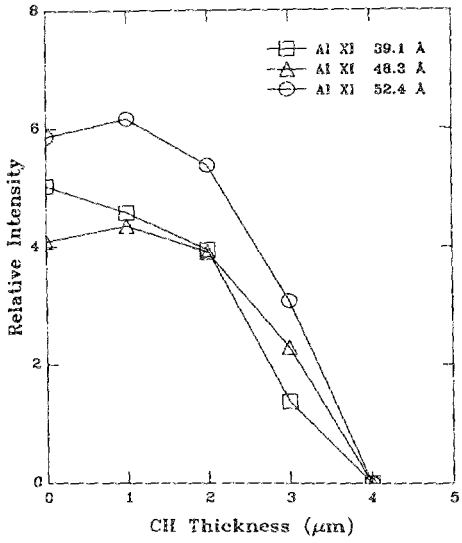

FIG. 10. LILAC hydro-code simulation of AlXI line intensities as a function of CH thickness. The experimentally measured laser intensity I_L is used here. The burnthrough depth is a factor of 2 lower than experiment.

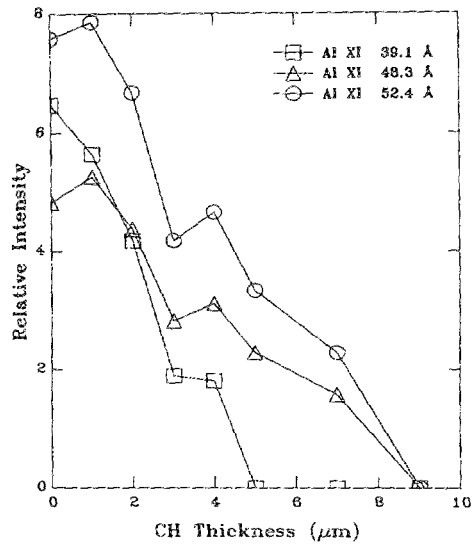

FIG. 12. LILAC simulation of AlXI burnthrough curve at three times the experimentally measured laser intensity. There is better agreement with experimental measurements of the burnthrough depth.

nonuniform irradiance of the laser onto the target, leading to "hot spots" which dominate the spectral emission.[16,17] These localized hot spots cover small regions (diameter $<20\,\mu m$) of the target and can have significantly higher irradiance than the measured average laser intensity. It has been observed that the onset time of x-ray signature lines are advanced by up to 100 ps from code predictions at nominal intensity. In order to agree with experimental onset times, it was determined by Delettrez *et al.*[17] that the simulation irradiance must be three times the nominal experimental value. This is consistent with significant laser energy (a few percent) existing at intensities equal to or larger than three times nominal.

By using an irradiance three times the experimental value to represent hot spots, there is good burnthrough depth agreement here between the simulations and the experiment. Note that, although the general shape of the burnthrough curve agrees with experiment, individual shots are not expected to be modeled accurately due to the difficulty of modeling laser nonuniformities. Figures 12 and 13 show simulations of AlXI and TiXX burnthrough curves at three times the nominal laser intensity using $f=0.1$. The burnthrough depth now matches the experimental measurements much better. Laser nonuniformities could also help explain the 1054-nm burnthrough results[14] and be a factor in explaining different experimental thermal transport results at different laboratories.

V. CONCLUSIONS

We have investigated electron thermal transport in 351-nm, laser-irradiated spherical targets. Spectroscopic measurements were made of emission lines from a lower-tem-

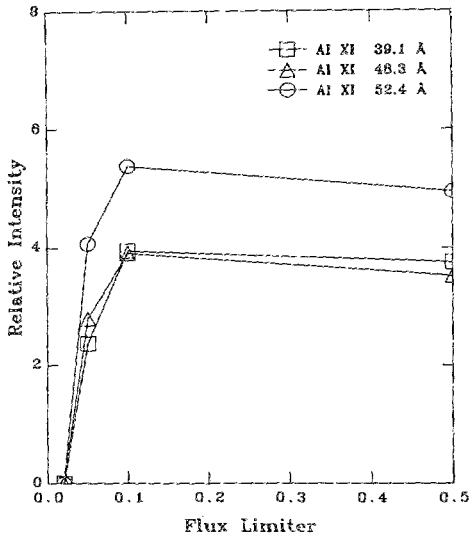

FIG. 11. LILAC simulation of AlXI line intensities as the flux limiter is varied.

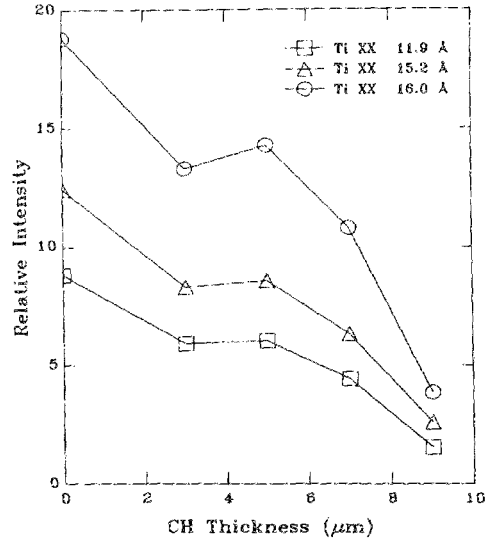

FIG. 13. LILAC simulation of TiXX burnthrough curve at three times the experimentally measured laser intensity.

perature region of the plasma than previously studied. No significant difference in thermal transport was observed for this plasma region indicating that the temperature profile is smoothly varying. In addition no evidence of a low-temperature foot or preheat was observed. The measured mass ablation rate was consistent with previous experiments at LLE using time-integrated x-ray measurements. Nonuniformities in laser irradiance had a major influence on comparisons between experimental measurements and hydrodynamic code calculations. A larger effective laser intensity was required in the hydrodynamic code to reach agreement with experiment.

ACKNOWLEDGMENTS

We would like to thank L. DaSilva, G. Gregory, E. Kowaluk, and W. Watson for technical assistance and J. Delettrez for useful discussions. We also thank U. Feldman and W. Behring for the use of the grazing incidence spectrograph. The research and materials incorporated in this work were partially developed at the National Laser Users Facility at the University of Rochester's Laboratory for Laser Energetics, with financial support from the U.S. Department of Energy through Contract No. DEAS08-86DP-10554. Targets used in this research were supplied by KMS Fusion, Inc. and by the University of Rochester Laser Fusion Feasibility Project.

[1]C. E. Max, C. F. McKee, and W. C. Mead, Phys. Fluids **23**, 1620 (1980).
[2]J. Delettrez, "Thermal Electron Transport in Direct-Drive ICF," UR/LLE Report No. 167 (August 1985).
[3]D. Duston, R. W. Clark, J. Davis, and J. P. Apruzese, Phys. Rev. A **27**, 1441 (1983).
[4]L. Spitzer and R. Härm, Phys. Rev. **89**, 972 (1953).
[5]R. C. Malone, R. L. McCrory, and R. L. Morse, Phys. Rev. Lett. **34**, 721 (1975).
[6]D. Shvarts, J. Delettrez, R. L. McCrory, and C. P. Verdon, Phys. Rev. Lett. **47**, 247 (1981).
[7]A. R. Bell, R. G. Evans, and D. J. Nicholas, Phys. Rev. Lett. **46**, 247 (1981).
[8]F. C. Young, R. R. Whitlock, R. Decoste, B. H. Ripin, D. J. Nagel, J. A. Stamper, J. M. McMahon, and S. E. Bodner, Appl. Phys. Lett. **30**, 45 (1977).
[9]B. Yaakobi, T. Boehly, P. Bourke, Y. Conturie, R. Craxton, J. Delettrez, J. Forsyth, R. Frankel, L. Goldman, R. McCrory, M. Richardson, W. Seka, D. Shvarts, and J. Soures, Opt. Comm. **39**, 175 (1981).
[10]M. H. Key, W. T. Toner, T. J. Goldsack, J. D. Kilkenny, S. A. Veats, P. F. Cunningham, and C. L. S. Lewis, Phys. Fluids **26**, 2011 (1983).
[11]T. J. Goldsack, J. D. Kilkenny, B. J. MacGowan, P. F. Cunningham, C. L. S. Lewis, M. H. Key, and P. T. Rumsby, Phys. Fluids **25**, 1634 (1982).
[12]J. A. Tarvin, W. B. Fechner, J. T. Larsen, P. D. Rockett, and D. C. Slater, Phys. Rev. Lett. **51**, 1355 (1983).
[13]A. Hauer, W. C. Mead, O. Willi, J. D. Kilkenny, D. K. Bradley, S. D. Tabatabei, and C. Hooker, Phys. Rev. Lett. **53**, 2563 (1984).
[14]B. Yaakobi, J. Delettrez, L. M. Goldman, R. L. McCrory, R. Marjoribanks, M. C. Richardson, D. Shvarts, S. Skupsky, J. M. Soures, C. Verdon, D. M. Villeneuve, T. Boehly, R. Hutchinson, and S. Letzring, Phys. Fluids **27**, 516 (1984).
[15]B. Yaakobi, O. Barnouin, J. Delettrez, L. M. Goldman, R. Marjoribanks, R. L. McCrory, M. C. Richardson, and J. M. Soures, J. Appl. Phys. **57**, 4354 (1985).
[16]P. A. Jaanimagi, J. Delettrez, B. L. Henke, and M. C. Richardson, Phys. Rev. A **34**, 1322 (1986).
[17]J. Delettrez, R. Epstein, M. C. Richardson, P. A. Jaanimagi, and B. L. Henke, Phys.Rev. A **36**, 3926 (1987).
[18]S. G. Noyes and H. Kim, J. Vac. Sci. Technol. A **3**, 1201 (1985).
[19]W. E. Behring, R. J. Ugiansky, and U. Feldman, Appl. Opt. **12**, 528 (1973).
[20]B. L. Henke and P. A. Jaanimagi, Rev. Sci. Instrum. **56**, 1537 (1985).
[21]LILAC, LLE Reports No. 16 (1973) and No. 36 (1976).